Available online at www.sciencedirect.com
SCIENCE DIRECT®
International Journal of Solids and Structures 43 (2006) 747–759
INTERNATIONAL JOURNAL OF SOLIDS and STRUCTURES
www.elsevier.com/locate/ijsolstr

Chaotic vibration of a nonlinear full-vehicle model

Qin Zhu [a,*], Mitsuaki Ishitobi [b]

[a] Department of Mechanical Engineering, Oyama National College of Technology, Nakakushi 771, Oyama 323-0806, Japan
[b] Department of Mechanical Engineering and Materials Science, Faculty of Engineering, Kumamoto University, 2-39-1 Kurokami, Kumamoto 860-8555, Japan

Received 7 October 2004; received in revised form 1 June 2005
Available online 6 October 2005

Abstract

The present work investigates the chaotic responses of a nonlinear seven degree-of-freedom ground vehicle model. The disturbances from the road are assumed to be sinusoid and the time delay between the disturbances is investigated. Numerical results show that the responses of the vehicle model could be chaotic. With the bifurcation phenomenon detected, the chaotic motion is confirmed with the dominant Lyapunov exponent. The results can be useful in dynamic design of a vehicle.

Keywords: Chaos; Nonlinear dynamics; Ground vehicle

1. Introduction

Since the vehicle dynamics is concerned with controllability and stability of automobile, it is important in design of a ground vehicle. The modeling of the vehicle with the analysis of the dynamic response of the mathematical model have been examined in a large number of previous investigations (Genta, 2003; Takahashi, 2003). In these studies, three typical models have been developed with researches related to the dynamic behavior of vehicle and its vibration control. The simplest representation of a ground vehicle is a quarter-car model with a spring and a damper connecting the body to a single wheel, which is in turn connected to the ground via the tire spring (Robson, 1979; Williams, 1997; Yang et al., 2001). As shown in Fig. 1(a), the mass representing the wheel, tire, brakes and part of the suspension linkage mass, is referred to as the unsprung mass. The quarter-car model is used only when the heave motion needs to be considered.

* Corresponding author.
E-mail address: zhu@oyama-ct.ac.jp (Q. Zhu).

0020-7683/$ - see front matter
doi:10.1016/j.ijsolstr.2005.06.070

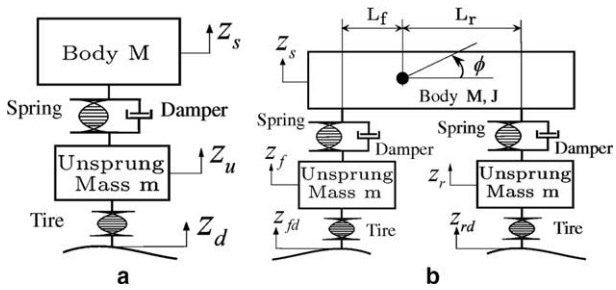

Fig. 1. Simplified vehicle model: (a) quarter-car model and (b) half-car model.

A half-car model is shown in Fig. 1(b). It is a two wheel model (front and rear) for studying the heave and pitch motions (Moran and Nagai, 1994; Vetturi et al., 1996; Campos et al., 1999). This four degree-of-freedom model allows the study of the heave and pitch motions with the deflection of tires and suspensions. Comparing to the full 3-D vehicle model, the half-car model is relatively simple to analyze and yet can reasonably predict the response of the system (Oueslati and Sankar, 1994). Therefore many researchers often use it. A more complex model is the full vehicle model which is a four wheel model with seven degree-of-freedom done for studying the heave, pitch and roll motions (Ikenaga et al., 2000).

In the studies of dynamic response of ground vehicle using these mechanical models, the spring and damper are usually assumed to be linear components for simplification. However, in practice an automobile is a nonlinear system because it consists of suspensions, tires and other components that have nonlinear properties. Therefore, the chaotic response may appear when the vehicle moves over a bumpy road. Since the chaotic responses is a random like motion, it could be harmful to the vehicle. By the lack of theoretical tool for predicting parameters in a system which induce chaotic response, the study of chaotic response for specified mechanical model is still needed. The main objective of the present study is investigate the chaotic response in a nonlinear seven degree-of-freedom vehicle. In Section 2, a nonlinear seven degree-of-freedom ground model is introduced and the motion equations of the system are derived. Next, the numerical simulation is conducted and the dynamic responses of the model are discussed. Frequency response diagrams, bifurcations and Poincaré maps are used to trace chaotic motion of the system. The dominant Lyapunov exponent is used to identify the chaos. The results indicate that the chaotic vibration exist as the forcing frequency is in the unstable region of the frequency response diagram of the system.

2. Simulation model

Fig. 2 shows the nonlinear full-vehicle model: the vehicle body is represented by a three degree-of-freedom rigid cuboid with mass m_s. The heave, pitch and roll motions of the sprung mass are considered. The four unsprung masses (front-left, front-right, rear-left and rear-right) are connected to each corner of the rigid cuboid. It is assumed that the four unsprung masses are free to bounce vertically. The suspensions between the sprung mass and unsprung masses are modeled as nonlinear spring and nonlinear dampers elements, while the tires are modeled as nonlinear springs with viscous damping.

It is assumed that the modeled nonlinear spring of suspension has following characteristics:

$$F_{sij} = k_{sij}\,\mathrm{sgn}(\Delta_{sij})|\Delta_{sij}|^{n_{sij}} \quad (i = f, r,\ j = \ell, r), \tag{1}$$

where F_{sij} is the spring dynamic force, k_{sij} is the equivalent stiffness, Δ_{sij} is the deformation of the spring and $\mathrm{sgn}(\cdot)$ is the signum function. The subscript s means spring of suspension, the subscript $i = f, r$ indicates the front and rear while the subscript $j = \ell, r$, indicates left and right. This way, F_{sfr}, k_{sfr} and Δ_{sfr} indicate the

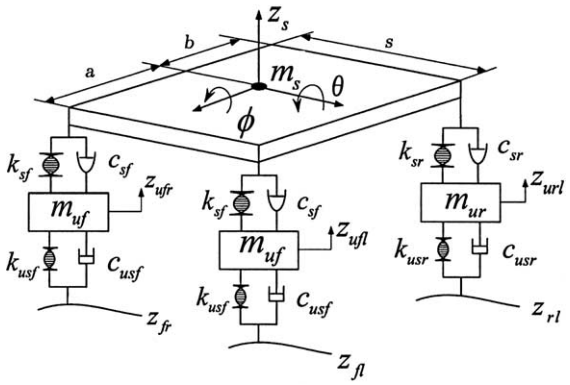

Fig. 2. Nonlinear full-vehicle model.

spring force, the equivalent stiffness and the deformation of suspension spring in front and right corner, respectively. In Eq. (1), n_{sij} is an exponent which represents nonlinearity of the spring and it is referred as the nonlinear coefficient. The unit of Δ_{sij} is in cm and k_{sij} in N/cm (Moran and Nagai, 1994). Since suspensions are usually arranged symmetrically along the longitudinal axis of the vehicle, Eq. (1) can be written as

$$F_{sij} = k_{si}\,\mathrm{sgn}(\Delta_{sij})|\Delta_{sij}|^{n_{si}} \quad (i = f, r,\ j = \ell, r). \tag{2}$$

The nonlinear damping forces of front and rear suspensions are given by

$$F_{cij} = c_{si}\dot{\Delta}_{uij} \quad (i = f, r,\ j = \ell, r), \tag{3}$$

where the subscript c indicates damping of suspension. F_{cij} is the damping force and $\dot{\Delta}_{uij}$ is the relative velocity between the extremes of the damper. The damping coefficient c_{si} is expressed by

$$c_{si} = \begin{cases} c_{sui} & \dot{\Delta}_{uij} \geqslant 0 \\ c_{sdi} & \dot{\Delta}_{uij} < 0 \end{cases} \quad (i = f, r,\ j = \ell, r), \tag{4}$$

where c_{sui} and c_{sdi} are damping coefficients for tension and compression, respectively.

The tire of the vehicle is also modeled by a nonlinear spring and the spring force is expressed in the same form as Eq. (2) but with a smaller value of nonlinear coefficient

$$F_{usij} = k_{usi}\,\mathrm{sgn}(\Delta_{usij})|\Delta_{usij}|^{n_{usi}} \quad (i = f, r,\ j = \ell, r), \tag{5}$$

where F_{usij} is the spring force, k_{usi} is the equivalent stiffness, Δ_{usij} is the deformation and n_{usi} is the nonlinear coefficient of the tire spring.

The damping of the tires is assumed to be viscous, thus the damping force is calculated as

$$F_{ucij} = c_{usi}\dot{\Delta}_{usij}, \tag{6}$$

where c_{usi} is the viscous damping coefficient and $\dot{\Delta}_{usij}$ is the relative velocity of extremes of the model of tires.

The sinusoid forcing function is used to describe the excitations caused by road surface. Thus the forcing function to tires in front-right, front-left, rear-right and rear-left are approximated by

$$z_{fr} = A\sin(2\pi ft), \tag{7}$$

$$z_{f\ell} = A\sin(2\pi ft + \beta), \tag{8}$$

$$z_{rr} = A\sin(2\pi ft + \alpha), \tag{9}$$

$$z_{r\ell} = A\sin(2\pi ft + \alpha + \beta), \tag{10}$$

where A and f are the amplitude and the frequency of the sinusoid road disturbance, respectively. The parameter β indicates the time delay between the forcing functions to two front tires, or to two rear tires, respectively. On the other hand, α indicates the time delay between the forcing functions to front-right and rear-right tires ((7) and (9)) or to front-left and rear-left tires ((8) and (10)), respectively.

After applying a force-balance analysis to the model in Fig. 2, the equations of motion can be derived to the static equilibrium positions.

Sprung mass:

$$m_{\mathrm{s}}\ddot{z}_{\mathrm{s}} = -F_{\mathrm{s}f\ell} - F_{\mathrm{c}f\ell} - F_{\mathrm{s}fr} - F_{\mathrm{c}fr} - F_{\mathrm{s}r\ell} - F_{\mathrm{c}r\ell} - F_{\mathrm{s}rr} - F_{\mathrm{c}rr} - m_{\mathrm{s}}g, \tag{11}$$

$$I_{\phi}\ddot{\phi} = \left(- F_{\mathrm{s}f\ell} - F_{\mathrm{c}f\ell} + F_{\mathrm{s}fr} + F_{\mathrm{c}fr} - F_{\mathrm{s}r\ell} - F_{\mathrm{c}r\ell} + F_{\mathrm{s}rr} + F_{\mathrm{c}rr}\right)\frac{s}{2}\cos\phi, \tag{12}$$

$$I_{\theta}\ddot{\theta} = \left(F_{\mathrm{s}f\ell} + F_{\mathrm{c}f\ell} + F_{\mathrm{s}fr} + F_{\mathrm{c}fr}\right)a\cos\theta - \left(F_{\mathrm{s}r\ell} + F_{\mathrm{c}r\ell} + F_{\mathrm{s}rr} + F_{\mathrm{c}rr}\right)b\cos\theta. \tag{13}$$

Front unsprung masses:

$$m_{\mathrm{u}f}\ddot{z}_{\mathrm{u}f\ell} = F_{\mathrm{s}f\ell} + F_{\mathrm{c}f\ell} - F_{\mathrm{us}f\ell} - F_{\mathrm{uc}f\ell} - m_{\mathrm{u}f}g, \tag{14}$$

$$m_{\mathrm{u}f}\ddot{z}_{\mathrm{u}fr} = F_{\mathrm{s}fr} + F_{\mathrm{c}fr} - F_{\mathrm{us}fr} - F_{\mathrm{uc}fr} - m_{\mathrm{u}f}g. \tag{15}$$

Rear unsprung masses:

$$m_{\mathrm{u}r}\ddot{z}_{\mathrm{u}r\ell} = F_{\mathrm{s}r\ell} + F_{\mathrm{c}r\ell} - F_{\mathrm{us}r\ell} - F_{\mathrm{uc}r\ell} - m_{\mathrm{u}r}g, \tag{16}$$

$$m_{\mathrm{u}r}\ddot{z}_{\mathrm{u}rr} = F_{\mathrm{s}rr} + F_{\mathrm{c}rr} - F_{\mathrm{us}rr} - F_{\mathrm{uc}rr} - m_{\mathrm{u}r}g. \tag{17}$$

The forces to the sprung mass in Eqs. (11)–(15) can be calculated as

$$F_{\mathrm{s}f\ell} = 100^{(n_{\mathrm{s}f}-1)}k_{\mathrm{s}f}\,\mathrm{sgn}(\Delta_{\mathrm{u}f\ell} - \Delta_{\mathrm{s}f})|\Delta_{\mathrm{u}f\ell} - \Delta_{\mathrm{s}f}|^{n_{\mathrm{s}f}}, \tag{18}$$

$$F_{\mathrm{s}fr} = 100^{(n_{\mathrm{s}f}-1)}k_{\mathrm{s}f}\,\mathrm{sgn}(\Delta_{\mathrm{u}fr} - \Delta_{\mathrm{s}f})|\Delta_{\mathrm{u}fr} - \Delta_{\mathrm{s}f}|^{n_{\mathrm{s}f}}, \tag{19}$$

$$F_{\mathrm{c}f\ell} = c_{\mathrm{s}f}\dot{\Delta}_{\mathrm{u}f\ell}, \tag{20}$$

$$F_{\mathrm{c}fr} = c_{\mathrm{s}f}\dot{\Delta}_{\mathrm{u}fr}, \tag{21}$$

$$F_{\mathrm{s}r\ell} = 100^{(n_{\mathrm{s}r}-1)}k_{\mathrm{s}r}\,\mathrm{sgn}(\Delta_{\mathrm{u}r\ell} - \Delta_{\mathrm{s}r})|\Delta_{\mathrm{u}r\ell} - \Delta_{\mathrm{s}r}|^{n_{\mathrm{s}r}}, \tag{22}$$

$$F_{\mathrm{s}rr} = 100^{(n_{\mathrm{s}r}-1)}k_{\mathrm{s}r}\,\mathrm{sgn}(\Delta_{\mathrm{u}rr} - \Delta_{\mathrm{s}r})|\Delta_{\mathrm{u}rr} - \Delta_{\mathrm{s}r}|^{n_{\mathrm{s}r}}, \tag{23}$$

$$F_{\mathrm{c}r\ell} = c_{\mathrm{s}r}\dot{\Delta}_{\mathrm{u}r\ell}, \tag{24}$$

$$F_{\mathrm{c}rr} = c_{\mathrm{s}r}\dot{\Delta}_{\mathrm{u}rr}, \tag{25}$$

where

$$\Delta_{\mathrm{u}f\ell} = \frac{s}{2}\sin\phi - a\sin\theta + z_{\mathrm{s}} - z_{\mathrm{u}f\ell}, \tag{26}$$

$$\Delta_{\mathrm{u}fr} = -\frac{s}{2}\sin\phi - a\sin\theta + z_{\mathrm{s}} - z_{\mathrm{u}fr}, \tag{27}$$

$$\Delta_{\mathrm{u}r\ell} = \frac{s}{2}\sin\phi + b\sin\theta + z_{\mathrm{s}} - z_{\mathrm{u}r\ell}, \tag{28}$$

$$\Delta_{\mathrm{u}rr} = -\frac{s}{2}\sin\phi + b\sin\theta + z_{\mathrm{s}} - z_{\mathrm{u}rr}, \tag{29}$$

$$\Delta_{\mathrm{s}r} = \left[\frac{a}{100^{(n_{\mathrm{s}r}-1)}k_{\mathrm{s}r}}\left(\frac{m_{\mathrm{s}}g}{2(a+b)}\right)\right]^{\frac{1}{n_{\mathrm{s}r}}}, \tag{30}$$

$$\Delta_{\mathrm{s}f} = \left[\frac{b}{100^{(n_{\mathrm{s}f}-1)}k_{\mathrm{s}f}}\left(\frac{m_{\mathrm{s}}g}{2(a+b)}\right)\right]^{\frac{1}{n_{\mathrm{s}f}}}. \tag{31}$$

The forces related to the unsprung mass in Eqs. (14)–(17) are expressed as

$$F_{\mathrm{us}f\ell} = 100^{(n_f-1)} k_{\mathrm{us}f}\,\mathrm{sgn}(\Delta_{\mathrm{us}f\ell} - \Delta_{\mathrm{su}f})|\Delta_{\mathrm{us}f\ell} - \Delta_{\mathrm{su}f}|^{n_{\mathrm{us}f}}, \tag{32}$$

$$F_{\mathrm{us}fr} = 100^{(n_f-1)} k_{\mathrm{us}f}\,\mathrm{sgn}(\Delta_{\mathrm{us}fr} - \Delta_{\mathrm{su}f})|\Delta_{\mathrm{us}fr} - \Delta_{\mathrm{su}f}|^{n_{\mathrm{us}f}}, \tag{33}$$

$$F_{\mathrm{uc}f\ell} = c_{\mathrm{us}f}\dot{\Delta}_{\mathrm{us}f\ell}, \tag{34}$$

$$F_{\mathrm{uc}fr} = c_{\mathrm{us}f}\dot{\Delta}_{\mathrm{us}fr}, \tag{35}$$

$$F_{\mathrm{us}r\ell} = 100^{(n_r-1)} k_{\mathrm{us}r}\,\mathrm{sgn}(\Delta_{\mathrm{us}r\ell} - \Delta_{\mathrm{su}r})|\Delta_{\mathrm{us}r\ell} - \Delta_{\mathrm{su}r}|^{n_{\mathrm{us}r}}, \tag{36}$$

$$F_{\mathrm{us}rr} = 100^{(n_r-1)} k_{\mathrm{us}r}\,\mathrm{sgn}(\Delta_{\mathrm{us}rr} - \Delta_{\mathrm{su}r})|\Delta_{\mathrm{us}rr} - \Delta_{\mathrm{su}r}|^{n_{\mathrm{us}r}}, \tag{37}$$

$$F_{\mathrm{uc}r\ell} = c_{\mathrm{us}r}\dot{\Delta}_{\mathrm{us}r\ell}, \tag{38}$$

$$F_{\mathrm{uc}rr} = c_{\mathrm{us}r}\dot{\Delta}_{\mathrm{us}rr}, \tag{39}$$

where

$$\Delta_{\mathrm{us}f\ell} = z_{\mathrm{u}f\ell} - A\sin(\omega t + \beta), \tag{40}$$

$$\Delta_{\mathrm{us}fr} = z_{\mathrm{u}fr} - A\sin(\omega t), \tag{41}$$

$$\Delta_{\mathrm{us}r\ell} = z_{\mathrm{u}r\ell} - A\sin(\omega t + \alpha + \beta), \tag{42}$$

$$\Delta_{\mathrm{us}rr} = z_{\mathrm{u}rr} - A\sin(\omega t + \alpha), \tag{43}$$

$$\Delta_{\mathrm{su}r} = \left[\frac{g}{100^{(n_r-1)}k_{\mathrm{su}r}}\left(\frac{m_{\mathrm{s}}a}{2(a+b)} + m_{\mathrm{u}r}\right)\right]^{\frac{1}{n_{\mathrm{us}r}}}, \tag{44}$$

$$\Delta_{\mathrm{su}f} = \left[\frac{g}{100^{(n_f-1)}k_{\mathrm{su}f}}\left(\frac{m_{\mathrm{s}}b}{2(a+b)} + m_{\mathrm{u}f}\right)\right]^{\frac{1}{n_{\mathrm{us}f}}}. \tag{45}$$

Table 1
Numerical values of the system parameters

Parameter	Value
Sprung mass, m_{s}	1500 kg
Roll axis moment of inertia, I_ϕ	460 kg m
Pitch axis moment of inertia, I_θ	2160 kg m
Front unsprung mass, $m_{\mathrm{u}f}$	59 kg
Rear unsprung mass, $m_{\mathrm{u}r}$	59 kg
Front suspension spring stiffness, $k_{\mathrm{s}f}$	35,000 N/m
Rear suspension spring stiffness, $k_{\mathrm{s}r}$	38,000 N/m
Nonlinear coefficient of suspension spring, $n_{\mathrm{s}f}$, $n_{\mathrm{s}r}$	1.5
Damping coefficient of front suspension, $c_{\mathrm{su}f}$	1000 N/m/s
Damping coefficient of front suspension, $c_{\mathrm{sd}f}$	720 N/m/s
Damping coefficient of rear suspension, $c_{\mathrm{su}r}$	1000 N/m/s
Damping coefficient of rear suspension, $c_{\mathrm{cd}r}$	720 N/m/s
Tire spring stiffness, $k_{\mathrm{us}f}$, $k_{\mathrm{us}r}$	190,000 N/m
Damping coefficient of tire, $c_{\mathrm{us}f}$, $c_{\mathrm{us}r}$	10 N/m/s
Nonlinear coefficient of tire spring, $n_{\mathrm{us}f}$, $n_{\mathrm{us}r}$	1.25
Length between the front of vehicle and the center of gravity of sprung mass, a	1.4 m
Length between the rear of vehicle and the center of gravity of sprung mass, b	1.7 m
Width of sprung mass, s	3 m

Owing to the high nonlinearity of the suspension spring and damping forces, the system behavior described by Eqs. (11)–(17) was studied numerically using the Runge–Kutta algorithm provided by MATLAB. In the computation, the absolute error tolerance was set to be lesser than 10^{-6}. Since numerical integration could give spurious results regarding the existence of chaos due to insufficient small time steps (Tongue, 1987), the step length was verified and it is ensure no such results were generated as a result of time discretization. The frequency response diagram, Poincaré maps and the dominant Lyapunov exponent were used to identify the chaotic response. The parameters of the vehicle model which are used in the numerical study are shown in Table 1.

3. Frequency response

In this section, the frequency response of the system is presented. The frequency response diagram, obtained by plotting the amplitude of the oscillating system versus the frequency of the excitation term, is often used to analyze the dynamics of a system (Belato et al., 2001). Since chaotic responses are possible when the forcing frequency is within an unstable region, shown in frequency response diagram (Zhu et al., 1994; Pust and Szöllös, 1999; Haller, 1997), then the forcing frequency for inducing chaos can be predicted by studying unstable regions in the frequency response diagram. For the full-vehicle model, the frequency response diagrams are plotted by defining the amplitude as the maximum absolute value of the amplitude of the displacement as in (Belato et al., 2001), and the frequency as frequency of the sinusoid road disturbance. Fig. 3 represents the resonance curves of the heave, roll and pitch motion of sprung mass and heave motion of unsprung mass in front-left corner when the forcing frequency f is slowly increased and then slowly decreased. The diagrams were calculated by using an increment $\Delta f = 0.001$ Hz as the variation of the control parameter. The forcing frequency was in the range of $0.01 \leqslant f \leqslant 10$ Hz. This parameter was changed 0.001 Hz with the time interval 50 s, so that the response diagrams can be presumed to be continuous.

Fig. 3(a) and (b) show the frequency response diagram of the heave motion for the sprung mass. When the forcing frequency is increasing, there are three jumps at $f = 3.51$ Hz, $f = 3.91$ Hz and $f = 4.82$ Hz, while between $f = 5.07$ Hz and $f = 5.39$ Hz the oscillations change into beats. As shown in Fig. 3(b), there are a small upward jump at $f = 4.76$ Hz and several small upward jumps around $f = 2.92$ Hz as the forcing frequency decreases. The beats begin at $f = 5.39$ Hz and end at $f = 5.07$ Hz. A new unstable region which does not exist as f is increasing appears in the forcing frequency $2.92 < f < 3.34$ Hz. Fig. 3(a) and (b) show that the numbers of jumps and unstable regions when forcing frequency is increasing are different from ones as forcing frequency is decreasing. This phenomenon was not observed in study of dynamic responses of four degree-of-freedom nonlinear half-car model or two degree-of-freedom nonlinear quarter-car model.

The frequency responses for roll motion of sprung mass are illustrated in Fig. 3(c) and (d). There is one unstable region in $5.09 < f < 5.39$ Hz when the frequency is increased. However, there are two unstable regions for decreasing frequency. One is in $5.07 < f < 5.39$ Hz, another is in $2.93 < f < 3.55$ Hz. Unlike the heave motion, there is only a small jump at 3.55 Hz for the decreasing frequency. Although the amplitude of the response is small, the existence of unstable region and jumps indicate that chaos in roll motion may exist.

The up and down jumps can be observed in frequency response diagram for the pitch motion of sprung mass shown in Fig. 3(e) as forcing frequency increases. There is one upward jump at $f = 3.51$ Hz, afterwards several downward jumps appear around $f = 3.91$ Hz. However, as shown in Fig. 3(f), there is only one upward jump at $f = 3.55$ Hz when forcing frequency decreases. Then, an unstable region with beats for pitch motion of sprung mass is in $5.09 < f < 5.40$ Hz for both cases, when the forcing frequency is increased and decreased. Periodic responses also change to beating oscillations in $2.90 < f < 3.30$ Hz when the

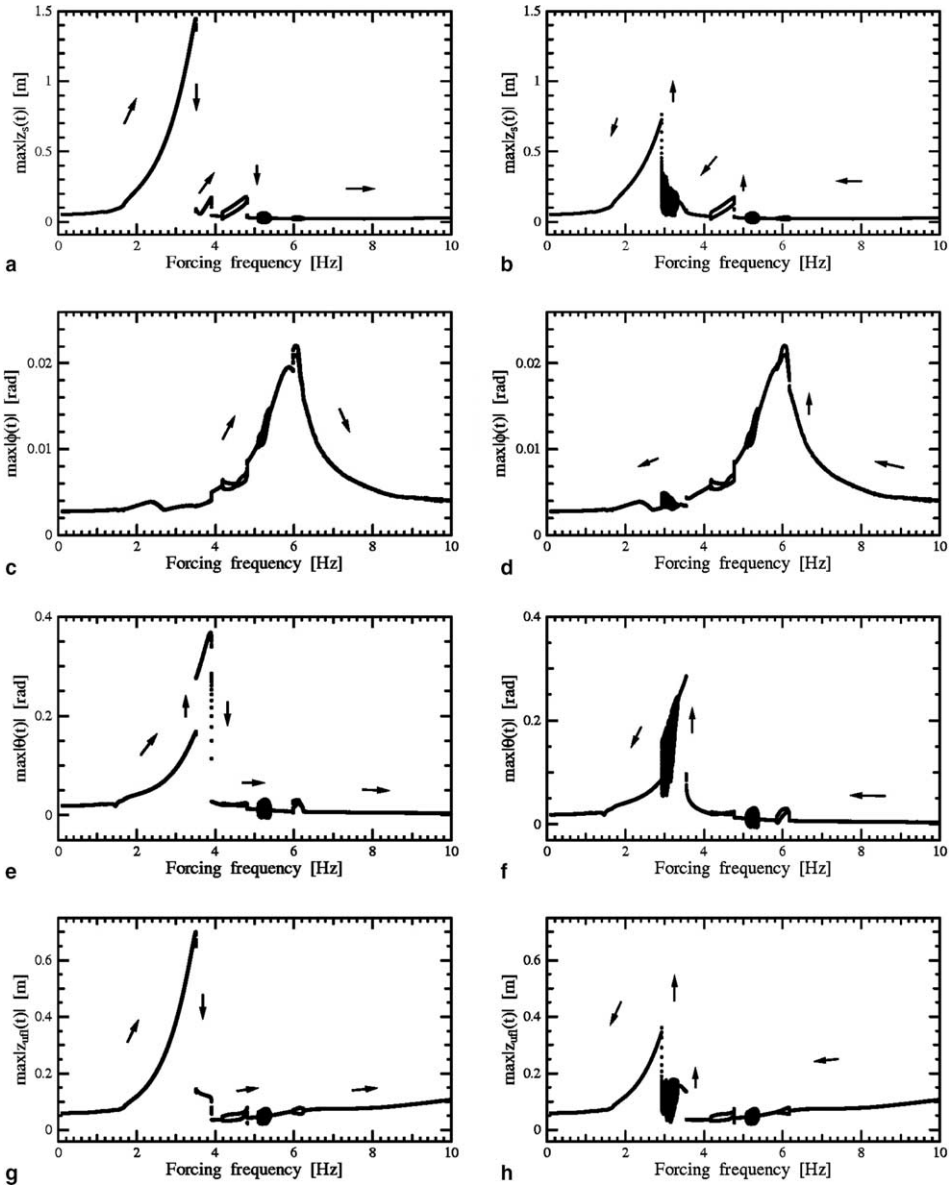

Fig. 3. Frequency response diagrams when the forcing frequency f is slowly increased and decreased ($A = 0.06$ m, $\beta = 9°$, $\alpha = 58°$, $0 < f < 10$ Hz): (a) and (b) $\max|z_s(t)|$; (c) and (d) $\max|\phi(t)|$; (e) and (f) $\max|\theta(t)|$; (g) and (h) $\max|z_{ufl}(t)|$.

frequency is decreasing. Therefore, there is one unstable region as the frequency is increased and two unstable regions as the frequency is decreased.

Since the frequency response diagrams of the four unsprung masses have the same characteristics, only the frequency response diagram of one in front-left is plotted in Fig. 3(g) and (h). When the forcing frequency is increased, one downward jump arises at $f = 3.51$ Hz. The periodic motion changes into beats between $f = 5.08$ Hz and $f = 5.40$ Hz, which is surrounded by two regions with period-2 solutions. When

the forcing frequency is decreased, there are one upward jump at $f = 3.55$ Hz and several small upward jumps around $f = 2.92$ Hz. Then there are two unstable regions, one is in $5.06 < f < 5.40$ Hz and another in $2.93 < f < 3.34$ Hz.

It is observed that the chaotic motion may not only appear as forcing frequency is within or near the unstable regions with beats, but also appear as forcing frequency is near one where the jump phenomenon is observed. Therefore, the response diagrams of the studied model in Fig. 3 show that chaotic

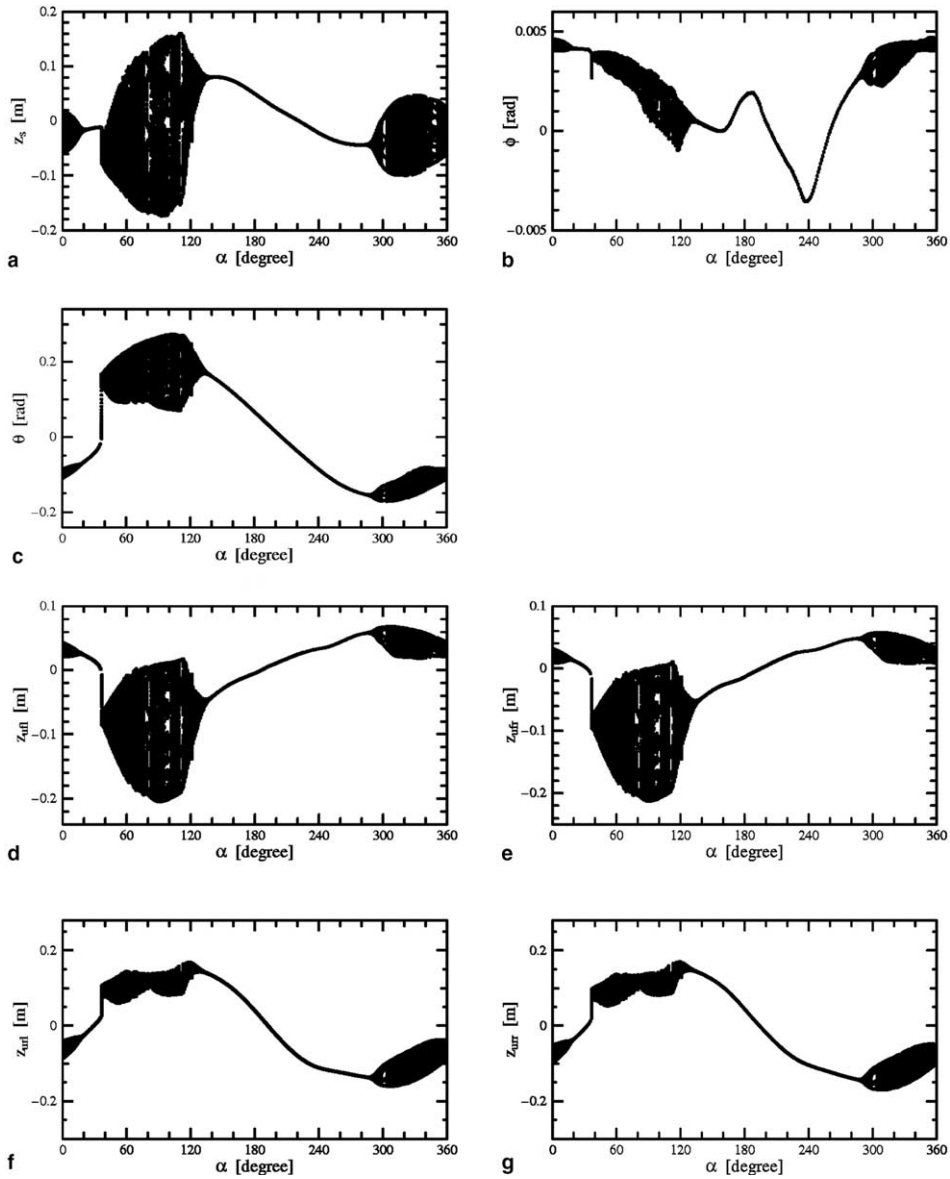

Fig. 4. Bifurcation diagrams obtained by varying α ($A = 0.06$ m, $f = 3.2$ Hz, $\beta = 9°$): (a) $z_s(t)$; (b) $\phi(t)$; (c) $\theta(t)$; (d) $z_{ufl}(t)$; (e) $z_{ufr}(t)$; (f) $z_{url}(t)$, and (g) $z_{urr}(t)$.

response is possible in the frequency regions described above, for some initial conditions and system parameters.

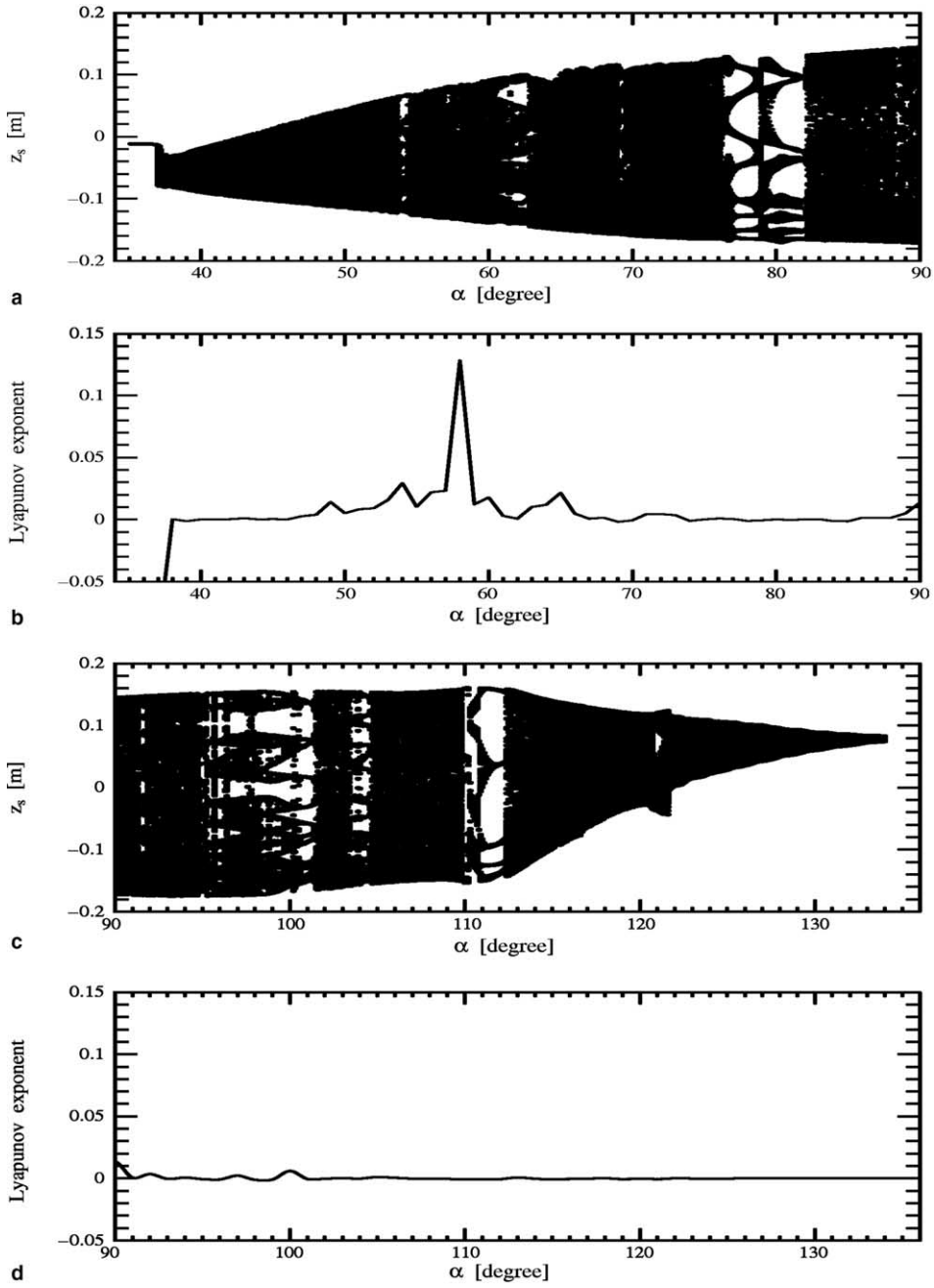

Fig. 5. Enlargements of Fig. 4(a) as $34° \leqslant \alpha \leqslant 136°$ and the corresponding the largest Lyapunov exponent.

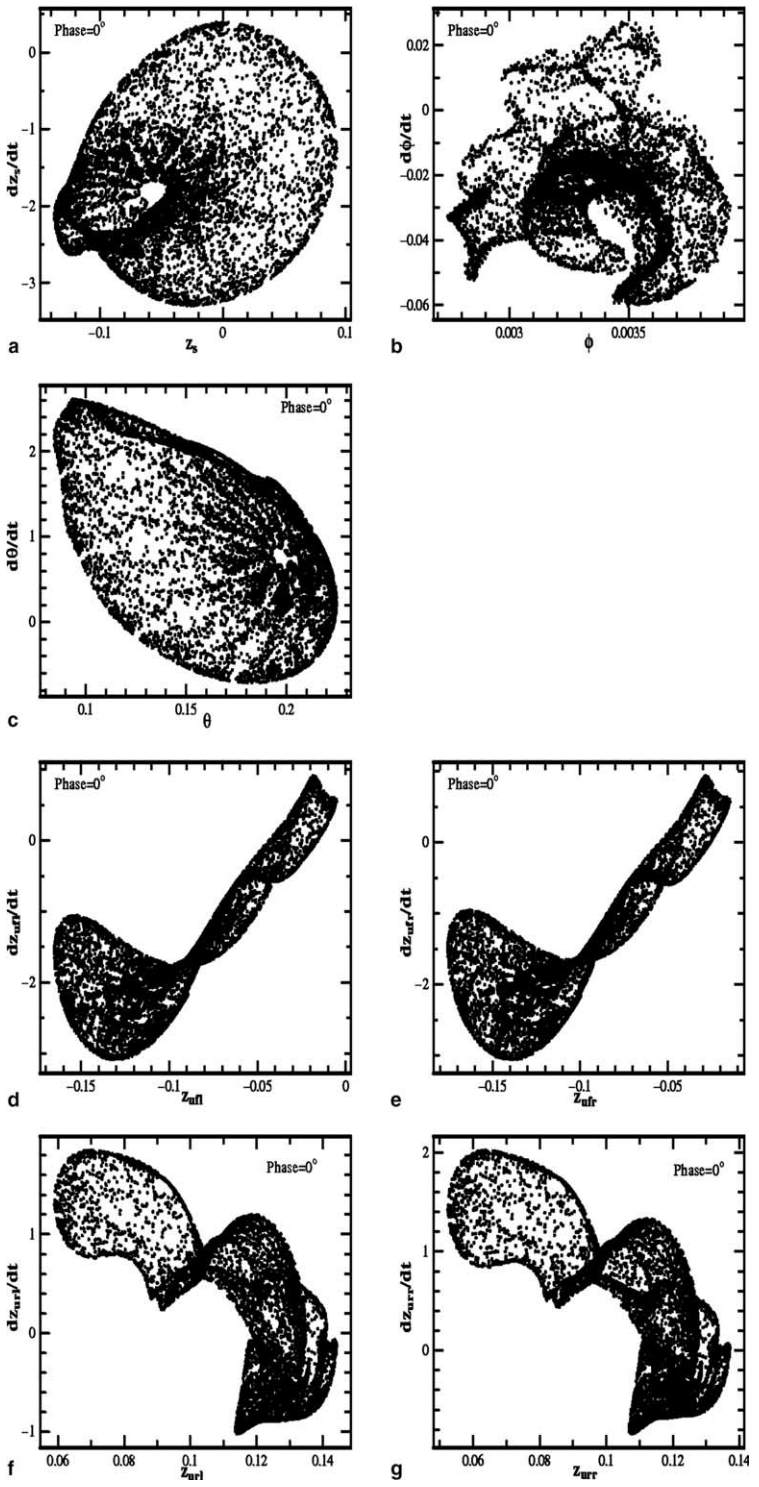

Fig. 6. Poincaré maps of chaotic motion of the system ($A = 0.06$ m, $f = 3.2$ Hz, $\beta = 9°$, $\alpha = 58°$).

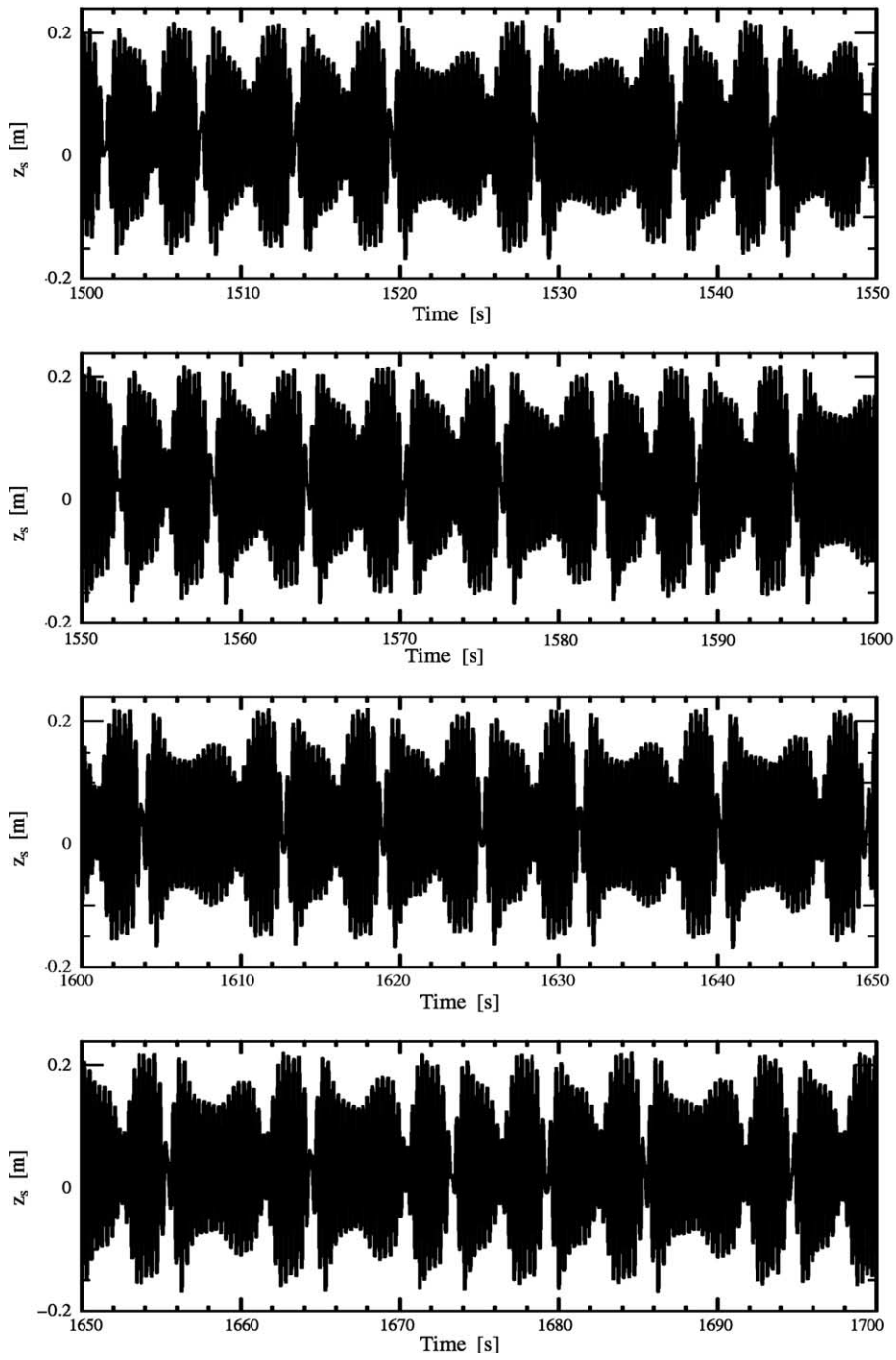

Fig. 7. Time response of chaotic motion of $z_s(t)$ ($A = 0.06$ m, $f = 3.2$ Hz, $\beta = 9°$, $\alpha = 58°$).

4. Bifurcation and chaos

In this section, the effect of the choice of the system parameters on the bifurcation structure are discussed. One of signals of impending chaotic behavior in dynamics systems is a series of changes in the nature of the periodic motions as some parameters are varied. The phenomenon of sudden change in the motion as a parameter is varied is called bifurcation (Moon, 1992). To make the bifurcation diagram, some measure of the motion is plotted as a function of a system parameter. In this paper, the bifurcation diagram is obtained by plotting the Poincaré points of the displacement concerning to one of the parameters of the system.

To investigate the effect of time delay α to the appearance of chaotic response, the bifurcation diagrams in $0^\circ \leqslant \alpha < 360^\circ$ were constructed via direct integration of the Eqs. (11)–(17). One of the results is shown in Fig. 4. The bifurcation diagrams of the system were obtained by plotting the Poincaré points of the response against the time delay α. The integration time was set to be 300 excitation cycles and only the last 100 Poincaré points were collected at each α. The parameters of excitation used in the computation were $A = 0.06$ m, $f = 3.2$ Hz and $\beta = 9^\circ$ and the initial conditions were set to zeros.

Fig. 4 indicates that the chaotic responses are possible as $0^\circ \leqslant \alpha \leqslant 20^\circ$, $38^\circ \leqslant \alpha \leqslant 136^\circ$ and $290^\circ \leqslant \alpha < 360^\circ$. It also shows that the responses of sprung mass and unsprung masses become chaotic simultaneously. An enlargement of the bifurcation diagram (Fig. 4(a), for $38^\circ \leqslant \alpha \leqslant 136^\circ$) is shown in Fig. 5(a) and (c), where periodic and chaotic motions were observed. The corresponding the largest Lyapunov exponent are shown in Fig. 5(b) and (d).

The Poincaré maps of the responses of the system when $\alpha = 58^\circ$ are shown in Fig. 6. Each Poincaré map contains 10,000 sampling points and shows the existence of strange attractors. To determine whether the time responses corresponding to Fig. 6 were chaotic, the Wolf's algorithm (Wolf et al., 1985) was used to calculate the dominant Lyapunov exponent. The time histories of the system from $t = 200$ s to $t = 1700$ s were used in the computation and the dominant Lyapunov exponents calculated were $\lambda_{z_s} = 0.128$, $\lambda_\phi = 0.001$, $\lambda_\theta = 0.013$, $\lambda_{z_{uf\ell}} = 0.087$, $\lambda_{z_{ufr}} = 0.043$, $\lambda_{z_{ur\ell}} = 0.501$ and $\lambda_{z_{urr}} = 0.172$ in the unit of bits/second. Fig. 7 shows the time response of $z_s(t)$. A direct look at the response suggests that the motion the mass m_s appears strange where the beats like motion appears randomly. These results indicated that the responses of the system were chaotic.

5. Conclusions

Chaotic responses and bifurcations of a nonlinear seven degree-of-freedom ground vehicle model which is subjected to sinusoid disturbance with time delay are studied through numerical simulation. It is found that, in frequency response diagrams, the number of unstable regions as the forcing frequency is increasing differentiates from one as the forcing frequency is decreasing. This is typical phenomenon for nonlinear dynamical systems, however the phenomenon was not observed in study of dynamic responses of two or four degree-of-freedom vehicle model. The increase of unstable regions in frequency response diagrams implies that there are more parameters for inducing chaotic motion because chaos usually appears as the forcing frequency is inside the unstable regions.

The results of numerical simulation also show that the chaotic response may appear in the unstable region of frequency response diagram. As there is variation of time delay in the road disturbances, the responses of the system may become chaotic. This result also implies that the chaotic vibration of the system could be avoided by making the possible frequency of excitation far from the unstable region in frequency response diagram.

References

Belato, D., Weber, H.I., Balthazar, J.M., Mook, M.D.T., 2001. Chaotic vibration of a nonideal electro-mechanical system. International Journal of Solids and Structures 38, 1699–1706.

Campos, J., Davis, L., Lewis, F.L., Ikenaga, S., Scully, S., Evans, M., 1999. Active suspension control of ground vehicle heave and pitch motions. In: Proceedings of the 7th IEEE Mediterranean Control Conference on Control and Automation, Haifa, Israel.

Genta, G., 2003. Motor Vehicle Dynamics, second ed. World Scientific, Singapore.

Haller, G., 1997. Chaos Near Resonance. Springer, New York.

Ikenaga, S., Lewis, F.L., Campos, J., Davis, L., 2000. Active suspension control of ground vehicle based on a full-vehicle model. In: Proceedings of American Control Conference, Chicago, USA.

Moon, F.C., 1992. Chaotic and Fractal Dynamics. John Wiley & Sons Inc.

Moran, A., Nagai, M., 1994. Optimal active control of nonlinear vehicle suspension using neural networks. JSME International Journal, Series C 37, 707–718.

Oueslati, F., Sankar, S., 1994. A class of semi-active suspension schemes for vehicle vibration control. Journal of Sound and Vibration 173, 391–411.

Pust, L., Szöllös, O., 1999. The forced chaotic and irregular oscillations of the nonlinear two degrees of freedom (2dof) system. International Journal of Bifurcation and Chaos 9, 479–491.

Robson, J.D., 1979. Road surface description and vehicle response. International Journal of Vehicle Design 9, 25–35.

Takahashi, T., 2003. Modeling, analysis and control methods for improving vehicle dynamic behavior (overview). R&D Review of Toyota CRDL 38, 1–9.

Tongue, B.H., 1987. Characteristics of numerical simulations of chaotic system. ASME Journal of Applied Mechanics 54, 695–699.

Vetturi, D., Gadola, M., Cambiaghi, D., Manzo, L., 1996. Semi-active strategies for racing car suspension control. SAE Technical Papers, No. 962553, II Motorsports Engineering Conference and Exposition, Dearborn, USA.

Williams, R.A., 1997. Automotive active suspensions, Part 1: Basic principles. Journal of Automobile Engineering, Part D 211, 415–426.

Wolf, A., Swift, J.B., Swinney, H.L., Vastano, J.A., 1985. Determining lyapunov exponents from a time series. Physica D 16, 285–317.

Yang, J., Suematsu, Y., Kang, Z., 2001. IEEE Transactions on Control Systems Technology 9, 295–317.

Zhu, Q., Tani, J., Takagi, T., 1994. Chaotic vibrations of a magnetically levitated system with two degrees of freedom. Journal of Technical Physics 35, 171–184.